

Properties of the diffuse X-ray background in a high-resolution hydrodynamical simulation

M. Roncarelli¹, L. Moscardini¹, P. Tozzi², S. Borgani^{3,4}, L.M. Cheng⁵, A. Diaferio⁶, K. Dolag⁷, G. Murante⁸

¹ Dipartimento di Astronomia, Università di Bologna, via Ranzani 1, I-40127 Bologna, Italy (mauro.roncarelli@unibo.it, lauro.moscardini@unibo.it)

² INAF, Osservatorio Astronomico di Trieste, via Tiepolo 11, I-34131 Trieste, Italy (tozzi@ts.astro.it)

³ Dipartimento di Astronomia, Università di Trieste, via Tiepolo 11, I-34131 Trieste, Italy (borgani@ts.astro.it)

⁴ INFN – National Institute for Nuclear Physics, Trieste, Italy

⁵ Institute of Theoretical Physics, Chinese Academy of Sciences, Beijing 100080, China (clm@itp.ac.cn)

⁶ Dipartimento di Fisica Generale “Amedeo Avogadro”, Università di Torino, via Giuria 1, I-10125 Torino, Italy (diaferio@ph.unito.it)

⁷ Max-Planck Institut fuer Astrophysik, Karl-Schwarzschild Strasse 1, D-85748 Garching, Germany (kdolag@mpa-garching.mpg.de)

⁸ INAF, Osservatorio Astronomico di Torino, Strada Osservatorio 20, I-10025 Pino Torinese, Italy (murante@to.astro.it)

2 December 2024

ABSTRACT

We study the properties of the diffuse X-ray background by using the results of a cosmological hydrodynamical simulation of the concordance Λ CDM model. The simulation follows gravitational dynamics and gasdynamics, including also a realistic treatment of physical processes like radiative cooling, star formation and supernova feedback. Using its outputs we produce a set of maps of the X-ray emission from the intergalactic medium up to high redshift. We find that the signal in the soft (0.5–2 keV) band is lognormally distributed with a mean intensity of about $4 \times 10^{-12} \text{ erg s}^{-1} \text{ cm}^{-2} \text{ deg}^{-2}$; approximately 40 per cent of the emission is contributed by warm-hot ($10^5 < T < 10^7 \text{ K}$) gas, and 90 per cent comes from structures with $z < 0.9$. Since the spectrum is soft, being provided mostly by intergalactic medium at low temperature, the total mean intensity in the hard (2–10 keV) X-ray band is smaller by a factor of about 4. In order to put constraints on the physical processes included in our simulation, we compare the observational upper limits for the soft X-ray emission from diffuse gas ($1.2 \pm 0.3 \times 10^{-12} \text{ erg s}^{-1} \text{ cm}^{-2} \text{ deg}^{-2}$) with our results. For this purpose we remove the contributions from observable virialized objects (groups and clusters of galaxies) from the simulated maps by adopting different detectability criteria which are calibrated by using the characteristics of objects observed by *Chandra* at intermediate redshifts. We show that the diffuse soft X-ray emission is consistent with the present observational upper limits. However, if future measurements will further reduce by a factor of 2 the level of the unresolved X-ray background, a more efficient feedback mechanism should be required to suppress the soft emission from gas residing within group-sized haloes and filaments.

Key words: diffuse radiation – intergalactic medium – hydrodynamics – galaxies: clusters: general – X-rays: general – cosmology – theory

1 INTRODUCTION

A general result of hydrodynamic simulations of cosmic structure formation is that during the formation of galaxy clusters via gravitational collapse, a large amount of gas is left outside of these structures at present time. An important fraction of the total baryons of the universe (40–50 per cent) undergoes a process of shock-heating that starts at $z \sim 2$ and brings it to an intermediate temperature (10^5 to 10^7 K): this gas phase is often referred as Warm-Hot Intergalactic Medium (WHIM) (see, e.g., Davé et al. 2001; Croft et al. 2001).

Simulations also show that these baryons are not uniformly distributed: they constitute a filamentary network linking the largest virialized objects, the so-called cosmic web (Bond et al. 1996). The existence of these structures is believed to be the solution of the missing baryon problem (see, e.g., Cen & Ostriker 1999), i.e. that more than half of normal matter is yet to be seen by instruments: in fact the density of filaments is expected to be very low and so their detection is made difficult because of their extremely low surface brightness and projection effects (see, however, some first claimed

detections in X-ray analyses: Zappacosta et al. 2002; Markevitch et al. 2003; Finoguenov et al. 2003). Anyway, the intermediate temperature of the cosmic web gas suggests that it can produce a non-negligible X-ray emission through thermal bremsstrahlung. Given the physical state of the gas, this emission is expected to mostly contribute as a diffuse background at soft energies.

It is now generally accepted that some of the observed cluster X-ray properties, like the scaling relations between mass, X-ray luminosity and temperature and their redshift evolution, the temperature profiles, or the entropy excess in the central regions of poor clusters and groups, cannot be reproduced by a simple model for gasdynamics based on gravitational heating (see the discussion in Rosati et al. 2002; Voit 2005, and references therein). In the attempt of explaining these discrepancies, new processes have been included in the models of cluster formation, largely increasing the complexity of the intracluster medium (ICM) physics: radiative cooling, energy feedback from supernovae (SN) and active galactic nuclei (AGN), thermal conduction, turbulence, magnetic fields, etc. (see, e.g., Bower 1997; Cavaliere et al. 1998; Balogh et al. 1999; Pearce et al. 2000; Bryan 2000; Tozzi & Norman 2001; Muanwong et al. 2001; Voit & Bryan 2001b; Babul et al. 2002; Voit et al. 2002; Tornatore et al. 2003; Jubelgas et al. 2004; Dolag et al. 2005; Di Matteo et al. 2005). All of these processes not only act inside virialized objects, like galaxy groups and clusters, but also on the diffuse gas component at low density and temperature. As a consequence, the expected X-ray emission from the cosmic web can sensitively change when the parameters describing the ICM physics are varied. For these reasons observational data on the soft X-ray background produced by diffuse gas can be used as a probe of these physical processes, as suggested by different authors (see, e.g., Voit & Bryan 2001a; Bryan & Voit 2001; Xue & Wu 2003).

Thanks to the latest generation of X-ray satellites *Chandra* and *XMM-Newton*, the observational picture about the cosmic X-ray background (hereafter XRB) in the soft (0.5-2 keV) energy band has become much clearer. Very deep pointed observations, like the 1-2 Ms *Chandra* Deep Fields (CDFs) (Giacconi et al. 2002; Alexander et al. 2003) and the Lockman Hole *XMM-Newton* data (Worsley et al. 2004), showed that the soft XRB is largely produced by individual discrete sources, mostly AGN. Recent estimates of the percentage of the resolved contribution range between 85 to 95 per cent (see, e.g., Bauer et al. 2004; Worsley et al. 2005). These results indirectly set a stringent upper limit to the diffuse background: approximately $(1.2 \pm 0.3) \times 10^{-12}$ erg s⁻¹ cm⁻² deg⁻² (see the discussion in Section 5.1).

The availability of these new observational constraints suggests to re-consider the problem of the soft X-ray emission from the cosmic web and its implications for the ICM physics by updating a similar analysis made by Croft et al. (2001). The main goal of this paper is to check the consistency of our model with these limits by making use of the outputs of a cosmological hydrodynamic simulation (Borgani et al. 2004), which, besides gravitational dynamics and gasdynamics, includes an advanced treatment of the ICM with radiative cooling, star formation and SN feedback. Our previous analyses (Borgani et al. 2004; Ettori et al. 2004; Diaferio et al. 2005) showed that the results of this simulation are in encouraging agreement with some of the most significant observed properties of clusters, such as the mass-temperature and the X-ray luminosity-temperature relations; however, the feedback mechanism appears not efficient enough to avoid the production of overluminous groups and poor clusters.

The paper is organized as follows. In Section 2 we describe the characteristics of the simulation used in the following analy-

sis and we present the procedure we applied to produce a set of maps starting from its outputs. The general statistical properties of the background in the soft (0.5-2 keV) and hard (2-10 keV) X-ray bands as extracted from these maps are discussed in Sections 3 and 4, respectively. In Section 5 we review the observational estimates of the contribution of diffuse gas to the soft XRB and we compare them to the results from our mock maps in order to obtain qualitative constraints to the modelization of the physical processes included in our hydrodynamical simulation. The final Section 6 is devoted to our conclusions.

2 THE MAP SIMULATIONS

2.1 The hydrodynamical simulation

The study of the properties of the diffuse X-ray emission from the large-scale structure of the universe and its comparison with the observations require the analysis of the contribution to the total emission integrated over redshift. Therefore we need to simulate all the volume of the past light-cone seen by an observer located at $z = 0$. The reconstruction of the light-cone has been obtained by using the outputs of a cosmological hydrodynamical simulation, which allowed us to produce simulated maps of the X-ray intensity. In more detail, we used the results of the simulation presented in Borgani et al. (2004), which assumes the concordance cosmological model, i.e a flat Λ CDM model, dominated by the presence of the cosmological constant ($\Omega_m = 0.3, \Omega_\Lambda = 0.7$), with a Hubble constant $H_0 = h$ 100 km s⁻¹Mpc⁻¹ with $h = 0.7$, and a baryon density $\Omega_b = 0.04$. The initial conditions correspond to the cold dark matter (CDM) power spectrum and have been normalized by assuming $\sigma_8 = 0.8$. The run was carried out with the TreeSPH code GADGET-2 (Springel et al. 2001; Springel 2005) following the evolution from $z = 49$ to $z = 0$ of 480³ dark matter (DM) particles and as many gas particles. The box size was fixed to $192h^{-1}$ Mpc, so the corresponding mass resolution is $m_{DM} = 4.62 \times 10^9 h^{-1} M_\odot$ and $m_{gas} = 6.93 \times 10^8 h^{-1} M_\odot$ for DM and gas particles, respectively. The Plummer-equivalent gravitational softening was set to $\epsilon = 7.5 h^{-1}$ kpc at $z = 0$, fixed in physical units since $z = 2$, while it was taken to be fixed in comoving units at higher redshift.

The simulation, besides gravity and non-radiative hydrodynamics, includes an accurate treatment of the processes that influence the physics of the intracluster medium, like star formation processes by adopting a sub-resolution multiphase model for the interstellar medium (Springel & Hernquist 2003), feedback from SN with the effect of weak galactic outflows, radiative gas cooling and the heating by a uniform, time-dependent, photoionizing UV background. This run produced a hundred outputs logarithmically equispaced in expansion factor between $z = 9$ and $z = 0$.

2.2 The map-making procedure

In order to build the maps for the X-ray emission from the structures contained inside the past light-cone, we follow the same technique adopted by Croft et al. (2001) (see also similar applications for maps of the Sunyaev-Zel'dovich effect, e.g. da Silva et al. 2001; Springel et al. 2001; White et al. 2002). The method is based on the replication of the original box volume along the line of sight. Since we are assuming a flat cosmological model, we use the comoving coordinates for the projection because the light trajectory is a straight line in this reference frame. We decided to simulate past light-cones reaching $z = 6$. Even if this maximum redshift

can appear large to still have a significant signal in the X-ray band (this will be confirmed by our following analysis in Section 3), this choice has been done to obtain at the same time maps for the thermal and kinetic Sunyaev-Zel'dovich effect (not discussed in this paper), for which there is a non-negligible contribution from high-redshift gas. The extension of the light-cone corresponds to a comoving distance of approximately $5,770 h^{-1}$ Mpc, so we need to stack about 30 times the simulation volume to reach this limit. In order to obtain a better redshift sampling, we decide to divide each box into 3 equal slices along the line of sight (each of them with a depth of $64 h^{-1}$ Mpc) and for all of them we choose the output of the simulation that better matches the redshift of the central point of the slice. This leads to have 91 slices covered by using 82 different snapshots.

The necessity of avoiding the repetition of the same structures along the line of sight requires a randomization of the boxes used to build our maps: since our simulation assumes periodic boundary conditions, for each box entering the light-cone we combine a process of random recentering of the coordinates and a 50 per cent probability of reflecting each axis. The slices belonging to the same box undergo the same randomization process to avoid spatial discontinuities between them: this allows to retain the whole information on the structures inside the box and to strongly reduce the loss of power on the larger scales. By varying the initial random seeds we are also able to obtain different light-cone reconstructions: we used this technique to produce ten different realizations that we use to assess the statistical robustness of our results.

In order to have maps covering a larger field of view, we decided to replicate the boxes 4 times across the line of sight starting from comoving distances larger than half of the light-cone extension (i.e. larger than about $2,900 h^{-1}$ Mpc, corresponding to $z > 1.4$). The strategy to pile up boxes is shown in Fig. 1. In this way we are able to obtain maps having a side of 3.78 deg. Every map contains 8,192 pixel per side: consequently our resolution is $1.66''$, roughly three times the resolution of the CDFs at the aim-point.

This paper will be focused on the study of the X-ray emission in the soft (0.5-2 keV) and hard (2-10 keV) bands of the spectrum. Therefore, we need to calculate the contribution of every gas particle that lies inside the light-cone volume. The X-ray luminosity of the i -th particle in a given band $[E_1, E_2]$, as measured at $z = 0$, is calculated as

$$L_{X,i} = (\mu m_p)^{-2} x_e m_i \rho_i \Lambda(T_i, Z_i, E'_1, E'_2), \quad (1)$$

where μ is the mean molecular weight in units of the proton mass m_p , x_e is the ratio between the number density of free electrons and hydrogen nuclei (n_e/n_H) and m_i and ρ_i are the particle mass and density, respectively. Since only the gas with $T > 10^5$ K gives significant contribution to the X-ray emission, we can safely assume full ionization in the hot component for all the particles: therefore the values of μ and x_e depend only on the metallicity (notice that $\mu = 0.588$ and $x_e = 1.158$ for zero metallicity). The cooling function Λ is computed by using the plasma emission model by Raymond & Smith (1977) as a function of the temperature (T_i) and metallicity (Z_i) of the particle and depends on the energy interval $[E'_1, E'_2]$ calculated considering the K -correction for redshift: $E'_{1,2} = E_{1,2}(1+z)$.

As we will discuss in the following section, a sizeable contribution to the soft X-ray background comes from relatively warm particles, with temperature below 10^7 K. At such temperatures, the emissivity from metal lines becomes non negligible and, therefore, one needs to account for their contribution. In its original imple-

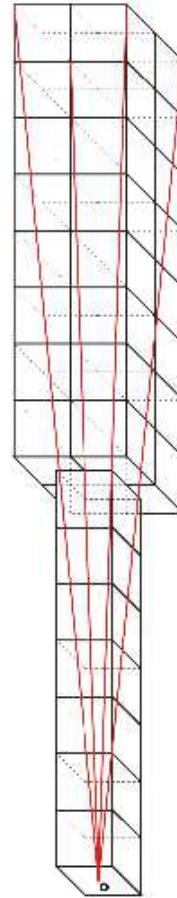


Figure 1. Sketch of the configuration adopted to realize the light-cone. The observer is located in the position O at the centre of the lowest side of the first box. The past light-cone is obtained by stacking the comoving volumes of the simulation outputs at the corresponding redshift. In order to obtain a larger field of view (3.78^2 deg 2), starting from $z = 1.4$ we decide to use four replications of the box. The red lines show the volume corresponding to the field of view inside the light-cone.

mentation, GADGET includes a prescription to generate metals from SN explosions. This model assumes that only SN-II contribute to the chemical enrichment, under the assumption of instantaneous recycling, i.e. metals are released at the same time of star formation, thus neglecting the effect of stellar life-times (see, e.g., Tornatore et al. 2004, for a more detailed implementation of chemical enrichment in GADGET). In Eq. (1) we adopt the resulting value Z_i of metallicity to compute the luminosity of each gas particle.

We then calculate the contribution of the i -th gas particle to the X-ray intensity $I_{X,i}$ as

$$I_{X,i} = L_{X,i} / (4\pi d_L(z)^2 A), \quad (2)$$

where $d_L(z)$ is the luminosity distance and A is the angular area covered by a pixel. This quantity is then distributed over the pixels by using an SPH smoothing kernel given by

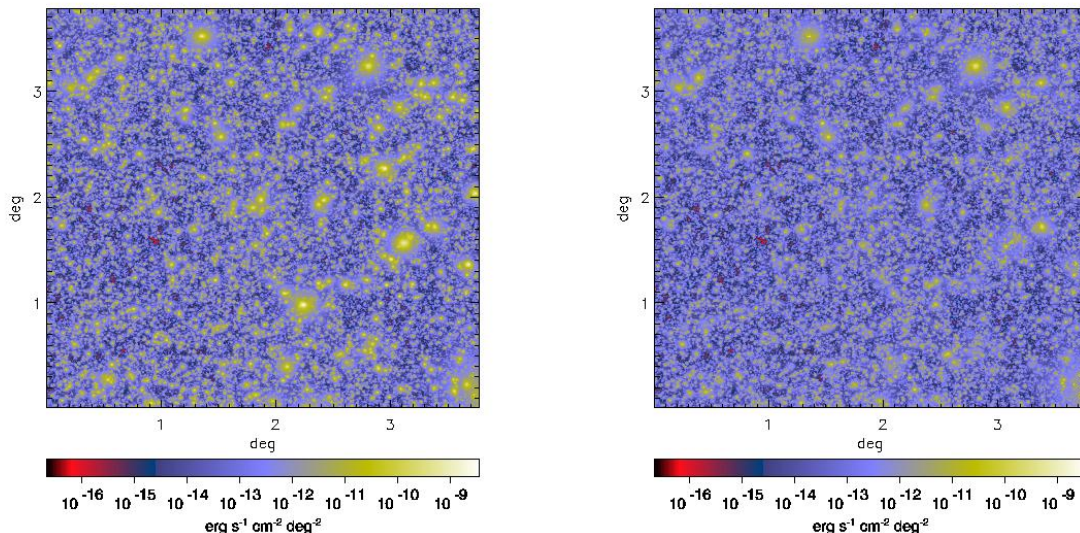


Figure 2. Maps of the soft (0.5-2 keV) X-ray intensity obtained by considering all the gas particles (IGM, left panel) and all the gas particles having a temperature in the range $10^5 < T < 10^7$ K (WHIM, right panel). The side corresponds to 3.78 deg and the pixel resolution is $1.66''$. These two maps refer to the same realization of the past light-cone.

$$W(x) \propto \begin{cases} 1 - 6x^2 + 6x^3, & 0 \leq x < 0.5 \\ 2(1-x)^3, & 0.5 < x \leq 1 \\ 0, & x > 1. \end{cases} \quad (3)$$

In the previous expressions it is $x \equiv \Delta\theta/\alpha_i$, where $\Delta\theta$ is the angular distance between the pixel centre and the projected particle position and α_i is the angle subtended by the particle smoothing length (also given by the hydrodynamical code). In order to conserve the total intensity contributed by each particle we normalize to unity the sum of the weights W over all “touched” pixels. Finally the intensity for a given pixel is obtained by summing over all the particles inside the light-cone.

To avoid spurious effects in the computation of the X-ray intensity we exclude those particles having a mean electron density $n_e > 0.26 h^2 \text{cm}^{-3}$. According to the model of Springel & Hernquist (2003) these particles are assumed to be composed by a hot ionized phase and a cold neutral phase, whose relative amounts depend on the local temperature and density. Since these particles are meant to account for the multi-phase nature of the interstellar medium, we decide here to exclude them from the computation of the X-ray emissivity.

3 THE PROPERTIES OF THE SOFT X-RAY BACKGROUND

Examples of intensity maps obtained by adopting the method described above are displayed in Fig. 2 for the emission in the soft (0.5-2 keV) band. Following Croft et al. (2001), we distinguish the X-ray contributions from the intergalactic medium (IGM, left panel), i.e. from all the gas particles, and from the warm-hot intergalactic medium (WHIM, right panel), defined as gas particles having a temperature between 10^5 and 10^7 K. The IGM map is dominated by several extended bright galaxy clusters (with flux in the range $10^{-12} - 10^{-11} \text{erg s}^{-1} \text{cm}^{-2}$) that give significant contribution to the total flux, but there is also a large number of smaller structures, corresponding to nearby galaxy groups or distant fainter

clusters. Since the WHIM maps do not contain the hottest particles, here these smaller objects give the dominating contribution, while the brightest galaxy clusters are much less prominent. Notice that, because of projection effects, neither map shows evident signatures of emission from filamentary structures.

The distribution of the values assumed by the intensity (considering the $1.66''$ pixels) is shown in Fig. 3 both for the IGM and the WHIM. The light lines refer to each of the ten light-cone realizations, while the heavy solid line shows their average. A small dispersion between the different realization is evident: this is mainly due to the inclusion in the maps of a larger or smaller number of galaxy clusters at relatively low redshifts. In general the two averaged distributions for $I \equiv \log I_x$ ($\text{erg s}^{-1} \text{cm}^{-2} \text{deg}^{-2}$) are very close to gaussian distributions. In particular we find $\bar{I} = -12.81$ with a corresponding r.m.s. of 1.05 for the IGM, and $\bar{I} = -13.01$ with a corresponding r.m.s. of 0.94 for the WHIM; the skewness is 0.30 and 0.25, for the IGM and the WHIM respectively. Of course the distributions differ for larger fluxes: this is due to the fact that the flux of the brightest structures comes from gas at high temperature.

The values for the intensity averaged on ten map realizations is reported in Table 1 for both the IGM and the WHIM. The quoted errors are the dispersions computed in fields of 1deg^2 to allow a direct comparison with the corresponding results reported in Croft et al. (2001). We find that the mean intensity for the IGM is about $4 \times 10^{-12} \text{erg s}^{-1} \text{cm}^{-2} \text{deg}^{-2}$, a factor 1.8 larger than in Croft et al. (2001). Also the corresponding dispersion is larger: about 50 per cent against about 20 per cent. Again, we checked that the high map-to-map spread is due to the presence of some bright galaxy clusters very close to the observer and giving a strong contribution to the total emission: this effect is also evident in the pixel distributions of separate maps shown in Fig. 3. Looking at the WHIM contribution, we find that its mean intensity is about 40 per cent of the total bremsstrahlung emission in the soft band (see Table 1). Again this value is larger than in the analysis of Croft et al. (2001), who reported a value of $4.15 \times 10^{-13} \text{erg s}^{-1} \text{cm}^{-2} \text{deg}^{-2}$, corresponding

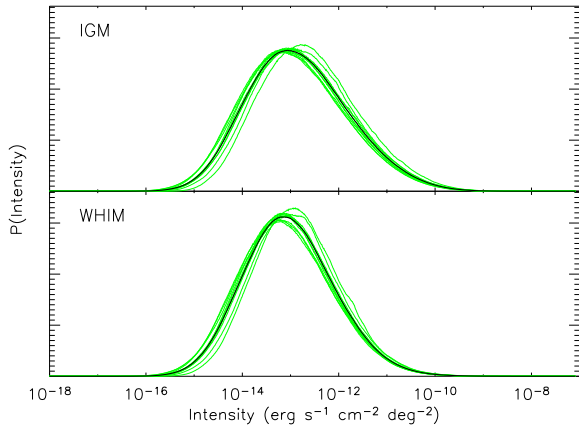


Figure 3. Distribution of pixel values for the intensity in the soft X-ray band. Upper and lower panels refer to the IGM and the WHIM, respectively. The light lines show the results for ten different realizations; the heavy solid line is the corresponding average.

Table 1. Average value of the intensity I_i in the two different X-ray bands for the IGM and the WHIM. The average is computed using ten different map realizations; the quoted errors are the r.m.s. in fields of 1 deg^2 .

Energy band	IGM (total) ($\text{erg s}^{-1} \text{ cm}^{-2} \text{ deg}^{-2}$)	WHIM ($\text{erg s}^{-1} \text{ cm}^{-2} \text{ deg}^{-2}$)
SOFT (0.5 - 2 keV)	$(4.06 \pm 2.19) \times 10^{-12}$	$(1.68 \pm 0.62) \times 10^{-12}$
HARD (2 - 10 keV)	$(1.01 \pm 1.53) \times 10^{-12}$	$(2.92 \pm 2.46) \times 10^{-14}$

to about 20 per cent of the total intensity of the IGM. We have to notice that the comparison between these results and those presented in Croft et al. (2001) can be only qualitative because the simulation analyzed in that paper considers a much smaller box ($50h^{-1}$ Mpc per side), assumes a slightly different cosmological model (a flat universe with $\Omega_m = 0.4$ and a primordial spectral index $n = 0.95$) and, most importantly, the included physical processes are not the same.

To determine which sources contribute most to the soft X-ray emission, in Fig. 4 we show how the mean intensity varies including only the pixels with fluxes above a given limit. The results show that the bremsstrahlung emission is dominated by very bright objects: pixels having a surface brightness larger than $10^{-10} \text{ erg s}^{-1} \text{ cm}^{-2} \text{ deg}^{-2}$ (mainly corresponding to galaxy clusters and groups) contribute to more than 50 per cent of the total value, both for the IGM and the WHIM.

In order to have an indication of the typical distances of the soft X-ray sources, following Croft et al. (2001) we compute for each pixel the mean redshift of the particles contributing to it, weighted by their fluxes. The resulting map for the same IGM realization shown in the left panel of Fig. 2 is displayed in Fig. 5 (left panel). Almost all the bright clusters are at low redshift ($z < 0.15$), while the emission from the faintest structures mainly comes from redshifts around unity. This is confirmed by the distributions of flux-weighted redshifts (central panel of Fig. 5), computed from the whole set of ten realizations: the shapes for the IGM and the WHIM are very similar, with a peak at $z \approx 0.7$. Notice that few re-

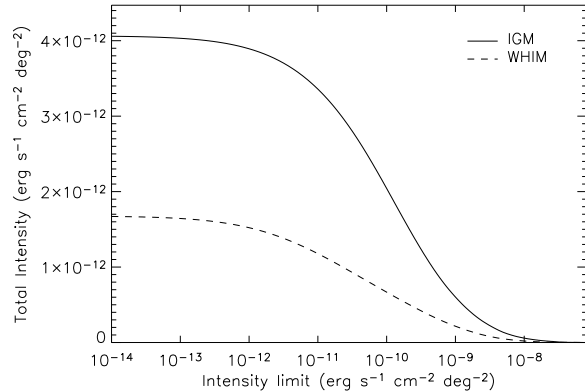


Figure 4. The value of the mean intensity (averaged over ten different map realizations) as a function of the lower limit of the pixel surface brightness. The solid and dashed lines refer to the IGM and the WHIM, respectively.

alizations have an excess of contribution from sources at relatively low redshift ($z < 0.15$): this is the reason of the large spread in the values for the mean intensity previously discussed. The analysis of the maps also clearly shows how the projection of nearby and distant objects makes it very difficult to see imprints of the filamentary network present in the large-scale structure of the universe. Finally, in the right panel of Fig. 5 we show the integrated soft X-ray intensity as a function of the limiting redshift. The curves both for the IGM and the WHIM reach half of the total value at $z \approx 0.3$, the 90 per cent level is reached around $z \approx 0.9$ for the IGM and at $z \approx 0.8$ for the WHIM. We can also notice that sources with $z > 2$ are contributing less than 1 per cent of the soft X-ray flux.

4 THE CONTRIBUTION IN THE HARD X-RAY BAND

It is well known that the hard (2-10 keV) X-ray band is strongly dominated by the emission from AGN. However, the small portion of gas at high temperature, mainly located inside the richest clusters, gives some contribution also in this band. The maps presented in Fig. 6 show the hard band intensity for the IGM and the WHIM (left and right panels, respectively) for the same light-cone realization shown in Fig. 2. We notice that, even if in some positions, corresponding to the hottest clusters, the intensity can reach values similar to those obtained in the soft X-ray maps ($10^{-9} \text{ erg s}^{-1} \text{ cm}^{-2} \text{ deg}^{-2}$), outside virialized regions the hard X-ray maps are much fainter. In the map for the WHIM the signal is strongly reduced and limited to the cluster atmospheres, with no evident emission from the diffuse gas: this makes the cosmic web not observable in this band because of its very low signal-to-noise ratio. However, the high contrast between clusters and diffuse regions of the hard band maps suggests an empirical way to identify the positions of galaxy clusters in our simulated maps. This method will be used in the following section to separate the emission coming from virialized objects from that produced by diffuse gas.

The small contribution of the IGM and the WHIM to the hard XRB is confirmed by the averaged total intensity reported in Table 1, for both components: we find about $1 \times 10^{-12} \text{ erg s}^{-1} \text{ cm}^{-2} \text{ deg}^{-2}$ and $3 \times 10^{-14} \text{ erg s}^{-1} \text{ cm}^{-2} \text{ deg}^{-2}$, for the IGM and the WHIM, respectively. These values account for approximately 25 per cent and 2 per cent of the corresponding mean intensity in the soft band. Notice that for the IGM our results agree very well with

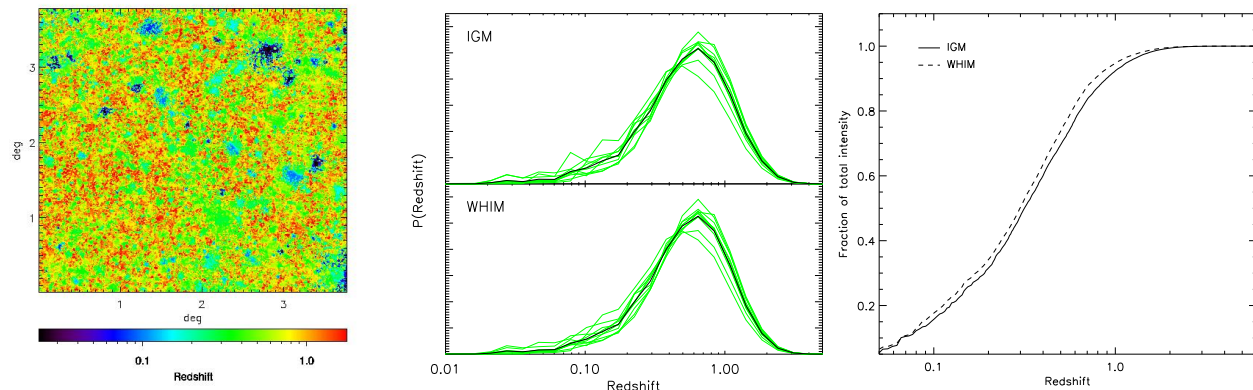


Figure 5. Left panel: the map of the flux-weighted redshift, computed for the IGM in the soft X-ray band. The plot refers to the same light-cone realization shown in Fig. 2. Central panel: as in Fig. 3, but for the distribution of the flux-weighted redshift in the soft X-ray band. Right panel: the integrated soft X-ray intensity (normalized to the total value) as a function of redshift. The solid and dashed lines refer to the IGM and the WHIM, respectively. The values plotted are the mean of ten map realizations.

the findings by Croft et al. (2001), while for the WHIM they are larger by a factor of 2. However, the field-to-field variance is quite large for the hard X-ray band, because most of the signal comes from nearby bright clusters: in fact the hard X-ray spectrum decreases in an exponential way and, even for hot objects, the bulk of the signal is rapidly shifted into the soft band for increasing redshifts.

A way to discriminate the AGN signal from that coming from clusters and cosmic web is based on the energy flux hardness ratio (HR), here defined as the ratio between the intensities in the hard and soft bands at each pixel position: $HR \equiv I_x[2 - 10\text{keV}] / I_x[0.5 - 2\text{keV}]$. The emission from AGN is in fact expected to have $HR > 0.5$, while much lower values are usual for galaxy clusters and diffuse gas. The map for the HR obtained from the same IGM realization shown in Figs. 2 and 6 is shown in the left panel of Fig. 7: in the plot it is easy to recognize the position of the richest galaxy clusters, while the connecting filamentary structure is almost completely absent. The distributions of the HR values for the ten realizations and their average are shown in the right panels, both for the IGM (up) and for the WHIM (low). In the former case the median value is around $HR = 0.03$, and less than few per cent of pixels have $HR > 0.5$; in the latter case the median is smaller than 0.01 and no pixel has $HR > 0.1$.

5 THE CONTRIBUTION OF DIFFUSE GAS TO THE SOFT X-RAY BACKGROUND

The goal of this section is to extract from the soft X-ray maps discussed above the contribution produced by the cosmic web, i.e. baryons which are not included in groups and clusters of galaxies which are currently identified in deep X-ray surveys. In order to check whether the modelization of the physical processes treated by our hydrodynamical simulation (which influence also the low-density gas regions) is reliable, the results will be compared with observational estimates (mainly upper limits). We have to notice that in the literature, as reviewed in the following subsection, there is no robust determination of the contribution to the soft XRB from diffuse gas: the value we will use later for comparison is based to some extent on interpretation of existing data.

5.1 Observational estimates

In the recent years, thanks to the availability of new X-ray satellites like *Chandra* and *XMM/Newton*, there have been many efforts to measure the total XRB and to resolve it in its different components (see, e.g. Giacconi et al. 2002; Moretti et al. 2002; Alexander et al. 2003; Worsley et al. 2004; Bauer et al. 2004, and references therein). In fact the possibility of recognizing the discrete sources which are giving the main contribution opens new windows to study the connection between AGN and galaxy formation and, most important for this work, puts constraints on possible diffuse signals.

At present the most reliable estimate of the total XRB in the soft (0.5-2 keV) band has been obtained by Worsley et al. (2005). By assuming the shape of the XRB in the [1-8 keV] band as found by De Luca & Molendi (2004) from *BeppoSAX* data, and taking into account the steepening of the spectrum below 1 keV as found in Roberts & Warwick (2001), they estimate an $\text{XRB}[0.5 - 2\text{keV}] = (8.12 \pm 0.23) \times 10^{-12} \text{ erg s}^{-1} \text{ cm}^{-2} \text{ deg}^{-2}$. Note that this value is larger than the one adopted by Bauer et al. (2004), who found $\text{XRB}[0.5 - 2\text{keV}] = (7.52 \pm 0.35) \times 10^{-12} \text{ erg s}^{-1} \text{ cm}^{-2} \text{ deg}^{-2}$. The discrepancy is originated by the fact that Bauer et al. (2004) extrapolate the hard spectrum in the soft band by assuming a slope of -1.4: of course, this does not take into account the steepening due to the non-AGN contribution, which, by the way, is the one we are most interested in. This total value includes any contribution, namely the Local Hot Bubble, the Galactic halo, unresolved galactic stars, and most important, the extragalactic components (both bright and faint) from point sources (AGN), clusters and groups and the truly diffuse gas. The XRB resolved so far in the soft band produced by these extragalactic sources has been recently estimated by Worsley et al. (2005), who found $(6.9 \pm 0.2) \times 10^{-12} \text{ erg s}^{-1} \text{ cm}^{-2} \text{ deg}^{-2}$. Similar results for the resolved component are presented by Bauer et al. (2004): $(6.7 \pm 0.3) \times 10^{-12} \text{ erg s}^{-1} \text{ cm}^{-2} \text{ deg}^{-2}$. Therefore, assuming the values found by Worsley et al. (2005) for the total XRB in the soft band, the emission which is still unresolved is approximately $(1.2 \pm 0.3) \times 10^{-12} \text{ erg s}^{-1} \text{ cm}^{-2} \text{ deg}^{-2}$. This figure represents an upper limit for the possible contribution from diffuse gas, since it still includes the unknown Galactic and Local contributions. Notice that the latter components are probably dominating the XRB below 0.5 keV, making highly uncertain the

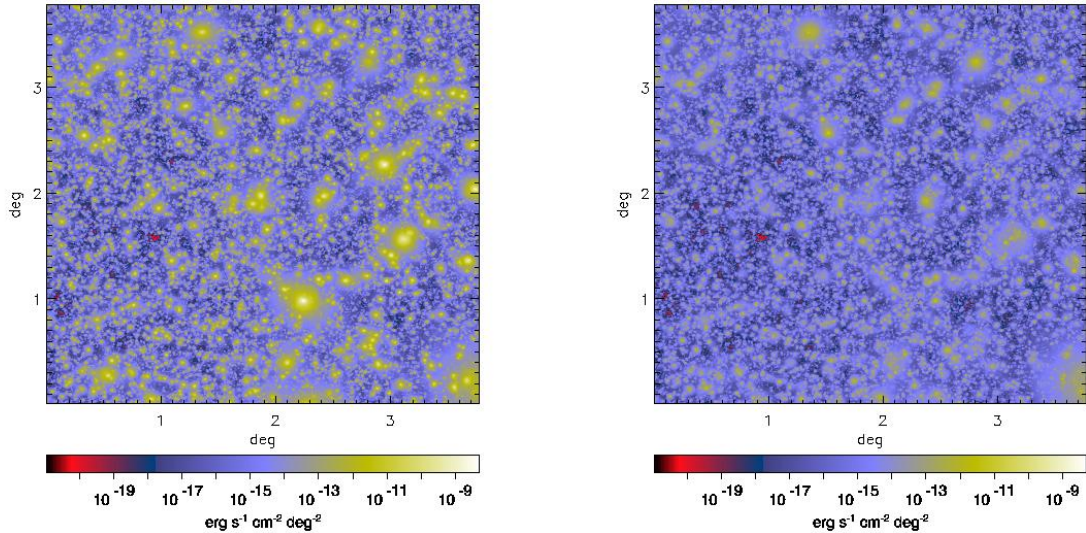


Figure 6. Maps of the hard (2-10 keV) X-ray intensity for the IGM and the WHIM (left and right panels, respectively). The side corresponds to 3.78 deg and the pixel resolution is $1.66''$. These maps have been obtained by the same light-cone realization shown in Fig. 2.

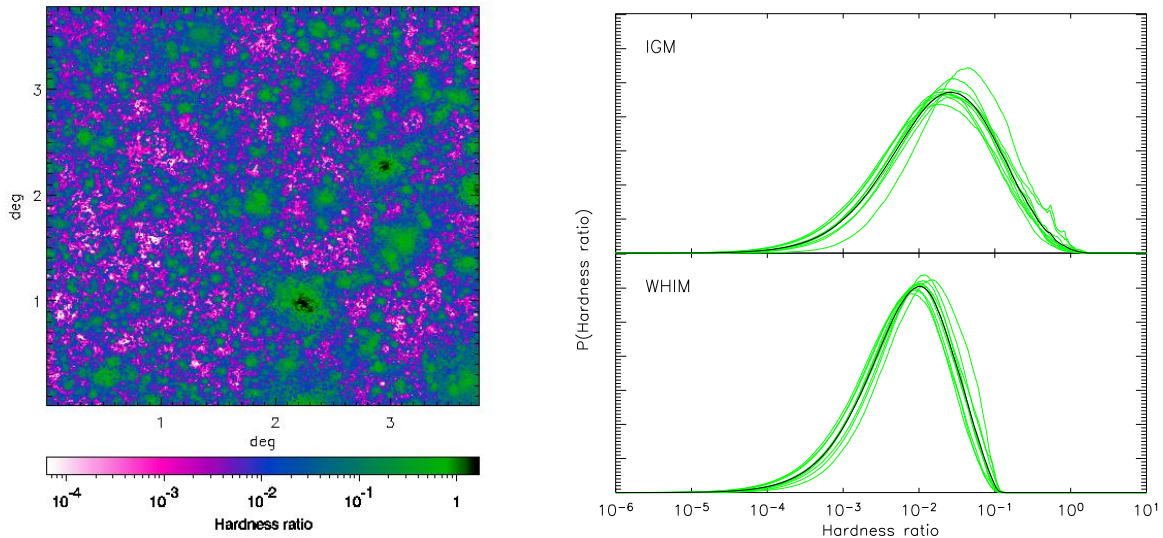


Figure 7. Left panel: the map for the hardness ratio (hard band to soft band) HR . This map is obtained from the same realization of the IGM light-cone shown in the left panels of Figs. 2 and 6. Right panels: distribution of HR for the IGM (up) and for the WHIM (low). The light lines show the results for ten different realizations; the heavy solid line is the corresponding average.

estimate of the extragalactic contribution in the lowest X-ray energy band, where the signal from the cosmic web is expected to be even more significant.

5.2 Subtracting the soft X-ray emission from virialized objects in the simulated maps

By comparing at face value the estimates of the IGM soft X-ray contribution reported in Table 1 to the observational data discussed above, we notice that it accounts for about 50 per cent of the total value of the XRB, but it is much larger (by a factor of 4) than the

upper limit left after resolving the discrete sources. Even considering the signal from the WHIM only, i.e. from gas having temperature between 10^5 and 10^7 K, the signal in our maps tends to be too large. However, this comparison is quite misleading, because in the results from the simulations is still included the portion of warm gas located in groups or in the external atmospheres of galaxy clusters, which is instead excluded in the reference observational value ($1.2 \pm 0.3 \times 10^{-12}$ erg s $^{-1}$ cm $^{-2}$ deg $^{-2}$). For this reason we need a more detailed analysis of our maps, where the virialized structures need to be excluded.

We already know from the previous analysis of our original

hydrodynamical simulation (see, e.g., Borgani et al. 2004) that the modelization of the included physical processes produces overluminous groups and poor clusters of galaxies. As discussed in that paper, additional sources of energy (like feedback from SN-Ia or AGN) would help in solving this discrepancy. This excess is located in high-density regions, whereas we are interested in the soft X-ray emission from the cosmic web: therefore, we need to identify and remove the X-ray extended sources, which correspond to galaxy clusters, from the total intensity of our maps.

The proper procedure would be to identify and remove all the clusters and groups from mock observations of our simulated volumes. In practice this is unfeasible, since it would require to simulate a full wide-area survey with all the related observational aspects, which is far beyond the aim of this paper. Therefore we will remove clusters and groups on the basis of their total flux as it appears on our flux maps. It is not trivial either, however, to find a reliable definition of the cluster and group regions to be applied to our bidimensional maps. For this reason we use a criterion based on the assumption of a surface brightness limit above which we consider that a map pixel belongs to a cluster region. In more detail, the steps of the procedure are as follows. First, we decide to make use of the results in the hard (2-10 keV) band because in that band the emission from diffuse gas is much lower and it is easier to identify the regions corresponding to virialized structures (see Fig. 6). Second, in order to define the threshold we consider a low-flux group identified in the CDF South (Giacconi et al. 2002) as a fiducial model for the lowest surface brightness objects that can be identified in the deepest X-ray exposures to date. This object (CDF5-594) is a group at $z \sim 0.7 - 0.8$: its emission is detected with a high signal-to-noise ratio over a circular region of approximately 2700 arcsec², after removing two point sources. After fitting its spectrum with a *mekal* model (see, e.g., Liedahl et al. 1995, and references therein) with Galactic absorption frozen to 9×10^{19} cm⁻², we obtain a temperature of about 2.1 keV. The corresponding *average* surface brightness in the hard (2-10 keV) band is 3.06×10^{-12} erg s⁻¹ cm⁻² deg⁻², which will be used as reference value in the following analysis. Comparable results have been obtained by considering a different galaxy group (CDF5-645), again identified in the CDF South exposure. Notice that this average value corresponds to the central part of the group (typically up to 3-4 core radii), then it represents an overestimate for the more external regions: for this reason, in the following analysis we will also consider as a threshold for the object identification values up to 8 times smaller. Finally, we need to consider also a threshold for the minimum angular size of the cluster region, in order to leave out bright regions which are smaller than the typical size of a galaxy group. For this purpose we take as a reference the physical length of 100 kpc, that corresponds to a minimum angular size of ~ 10 arcsec (at $z \sim 1$) for the cosmological model assumed in the simulation: this gives an angular surface of ~ 310 arcsec².

5.3 The soft X-ray emission from the cosmic web in the simulated maps

By applying the previously discussed thresholds in surface brightness and size on the maps produced in the hard (2-10 keV) X-ray band, we create a catalogue of connected regions corresponding to the virialized objects. We use them as a mask on the soft (0.5-2 keV) X-ray maps to remove their emission and finally obtain the diffuse contribution. By averaging on our ten different realizations, we find that the signal from diffuse gas corresponds to a value of 1.57×10^{-12} erg s⁻¹ cm⁻² deg⁻² which is comparable to the ob-

servational upper limit. The 69 per cent of the diffuse emission is coming from gas with temperature in the range $10^5 - 10^7$ K, while the total contribution of clusters and groups to the XRB is 2.49×10^{-12} erg s⁻¹ cm⁻² deg⁻², which is larger than the total contribution from clusters and groups as estimated from the observed number counts (Rosati et al. 2002, see also the corresponding discussion at the end of this section). As discussed above, the adopted surface brightness threshold can be considered as an average of the group emission at intermediate redshifts, and then it could be too high to account for all clusters' and groups' emission. In fact we find that 31 per cent of the 1.57×10^{-12} erg s⁻¹ cm⁻² deg⁻² emission is still produced by gas having a temperature larger than 10^7 K. This is further confirmed by a visual inspection of the masked maps: the external regions of nearby clusters are not excluded. This is an indication that in general the surface brightness threshold defining high density regions associated to groups and clusters of galaxies is likely lower than the adopted value. For this reason we repeat the previous analysis by using a threshold which is smaller by factors of 2, 4 and 8. The results, reported in Table 2, show a reduction of the contribution of diffuse gas by a factor of 2 when the surface brightness cut is 8 times smaller; the corresponding fraction of signal from the WHIM increases up to 82 per cent. In general we can conclude that the soft X-ray emission from diffuse gas computed from our simulation is consistent with the upper limit coming from observational data. The feedback model we are assuming is more efficient in the WHIM and/or in regions at intermediate density, even when it can show problems in the deepest potential wells.

Finally, as a self-consistency check, we compute the $\log N$ - $\log S$ function (always in the soft X-ray band) for our connected regions. The results are shown in Fig. 8 for the four different thresholds reported in Table 2. Again, we notice the excess with respect to the observational data, represented by a combination of data made by Rosati et al. (2002) and coming from *Rosat* Deep Cluster Survey (Rosati et al. 1998), EMSS (Rosati et al. 1995), BCS (Ebeling et al. 1998) and REFLEX (Boehringer et al. 2001). This excess is produced by the overluminous objects present in our simulation: only by lowering the threshold it is possible to match the counts suggested by the analysis of the CDF North and South.

6 CONCLUSIONS

In this paper we have used a cosmological hydrodynamical simulation of a concordance model Λ CDM to discuss the properties of the diffuse XRB. The simulation (Borgani et al. 2004) allows a realistic representation of many relevant physical processes affecting the gas component. Indeed the numerical treatment accounts for a time-dependent, photoionizing UV uniform background, radiative cooling processes within an optically thin gas of hydrogen and helium in collisional ionization equilibrium, star formation events and feedback processes from both SN-II and galactic winds. Our previous analyses (Borgani et al. 2004; Etori et al. 2004) showed that the results of this simulation are consistent with several observational X-ray properties of galaxy clusters. However, there are also a number of discrepancies that remain unaccounted for: in particular the cluster X-ray luminosity-temperature relation extracted from our simulation appears too high, i.e. there are overluminous groups and small clusters.

As suggested by different authors (see, e.g., Voit & Bryan 2001a; Bryan & Voit 2001; Xue & Wu 2003), an alternative way for constraining the model describing the thermal properties of baryons

Table 2. Contribution to the soft (0.5-2 keV) XRB from virialized objects (Column 2) and diffuse gas (Column 3) as a function of the adopted threshold for the surface brightness (Column 1). We also report the percentage of the diffuse contribution coming from the WHIM (Column 4). The quoted errors are the r.m.s. in fields of 1 deg². All values are in units of 10⁻¹² erg s⁻¹ cm⁻² deg⁻².

SOFT (0.5-2 KEV) X-RAY BACKGROUND (10 ⁻¹² erg s ⁻¹ cm ⁻² deg ⁻²)			
SURFACE BRIGHTNESS THRESHOLD IN THE HARD (2-10 KEV) X-RAY BAND	CONTRIBUTIONS FROM		
	VIRIALIZED OBJECTS	DIFFUSE GAS	% WHIM
3.06	2.49 ± 2.04	1.57 ± 0.27	(69 ± 13)%
1.53	2.78 ± 2.10	1.28 ± 0.19	(73 ± 12)%
0.77	3.05 ± 2.14	1.01 ± 0.13	(78 ± 11)%
0.38	3.28 ± 2.17	0.78 ± 0.09	(82 ± 11)%
OBSERVATIONAL UPPER LIMIT		1.2 ± 0.3	

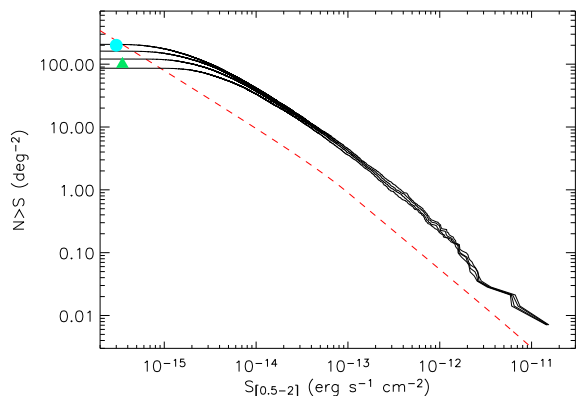


Figure 8. Number of objects as a function of the limiting flux in the soft (0.5-2 keV) X-ray band. The black solid lines are the results obtained considering the connected regions with 4 different surface brightness cuts (see Table 2 for the adopted values). As a reference we show (red dashed line) the observational data obtained by Rosati et al. (2002) by combining the results from the *Rosat* Deep Cluster Survey (Rosati et al. 1998), EMSS (Rosati et al. 1995), BCS (Ebeling et al. 1998) and REFLEX (Boehringer et al. 2001). At low fluxes we also report the values from the CDF North (cyan circle) and South (green triangle), as reported by Rosati et al. (2002).

and their cosmic history is related to the soft X-ray emission from diffuse gas. Indeed, a model for heating and cooling of the intracluster medium makes predictions in terms of diffuse emission from filaments and unresolved structures and thus can be compared to observational measurements of the XRB, which are now available (in form of upper limits), thanks to the deep *Chandra* data.

In order to test the model included in our simulation, starting from its outputs at different redshifts we realized a set of ten different maps, having a side of 3.78 deg and recovering the structures in the past light-cone up to $z = 6$ by following the same method adopted by Croft et al. (2001). The present analysis represents an extension of similar previous works, thanks to a much larger volume sampling, to a more realistic representation of the physical processes affecting the baryon history and to the comparison with the observed XRB data after the *Chandra* era.

The main results obtained by using our set of maps are as follows.

- The mean intensity for the IGM in the soft (0.5-2 keV) X-ray band is about 4.1×10^{-12} erg s⁻¹ cm⁻² deg⁻²; when considering

the WHIM (defined as gas with temperature between 10⁵ and 10⁷ K) the mean intensity reduces to about 1.7×10^{-12} erg s⁻¹ cm⁻² deg⁻². The distribution of the intensity in the maps is very similar to a lognormal. The 90 per cent of the signal comes from structures with $z < 0.9$.

- As expected, in the hard (2-10 keV) X-ray band the total mean intensity is smaller (by a factor 4) than in the soft one and becomes almost negligible when considering the WHIM (about 3×10^{-14} erg s⁻¹ cm⁻² deg⁻²). The hardness ratio in the maps has a distribution peaked on low values, with a median close to 0.03, which allows an easy discrimination with respect to the AGN signal.

- The soft X-ray emission from diffuse gas computed from our simulation after removing from the previous maps the regions corresponding to virialized objects is in general consistent with the present upper limit coming from observational data: $(1.2 \pm 0.3) \times 10^{-12}$ erg s⁻¹ cm⁻² deg⁻². This value has been estimated by removing the contribution from resolved sources (AGN, groups and clusters of galaxies) from the total XRB recently obtained by Worsley et al. (2005).

The last result shows that the physical processes here discussed are reproducing the X-ray properties of the warm-hot baryons. However, if in the near future the measurements of the possible contribution from Galactic and local structures (still included in the observational upper limits) will reduce the maximum allowed emission from the diffuse gas by a factor of 2, our predictions will start to conflict with the data. In this case a more efficient mechanism of feedback acting also on gas with intermediate temperatures and densities will be required.

As a conclusion, we confirmed that the comparison between observational constraints on the diffuse emission in the soft X-ray band and results from cosmological hydrodynamical simulations allows to gain information on the thermodynamical history of diffuse baryons. For the same reason it will be interesting in the future to study some detailed simulated observations of the diffuse gas to check its detectability via (emission and/or absorption) oxygen lines (OVII, OVIII and OVIX): for this purpose some dedicated wide-field high-resolution spectroscopic experiments are now in project. Another possibility could be to use the next generation of X-ray spectroscopic satellites, like *Constellation-X/XEUS* or *NEXT*, provided that their field of view is large enough (30' - 1 deg) to cover the filamentary structure.

ACKNOWLEDGEMENTS

Computations have been performed by using the IBM-SP4 at CINECA, Bologna, with CPU time assigned under an INAF-CINECA grant. This work has been partially supported by the PD-51 INFN grant. We are grateful to C. Gheller for his assistance. We acknowledge useful discussions with S. Etori, M. Galeazzi, P. Mazzotta, V. Springel, G. Tormen, L. Tornatore and E. Ursino.

REFERENCES

- Alexander D. M., et al., 2003, *AJ*, 126, 539
 Babul A., Balogh M. L., Lewis G. F., Poole G. B., 2002, *MNRAS*, 330, 329
 Balogh M. L., Babul A., Patton D. R., 1999, *MNRAS*, 307, 463
 Bauer F. E., Alexander D. M., Brandt W. N., Schneider D. P., Treister E., Hornschemeier A. E., Garmire G. P., 2004, *AJ*, 128, 2048
 Boehringer H., et al., 2001, *A&A*, 369, 826
 Bond J. R., Kofman L., Pogossyan D., 1996, *Nat*, 380, 603
 Borgani S., et al., 2004, *MNRAS*, 348, 1078
 Bower R. G., 1997, *MNRAS*, 288, 355
 Bryan G. L., 2000, *ApJ*, 544, L1
 Bryan G. L., Voit G. M., 2001, *ApJ*, 556, 590
 Cavaliere A., Menci N., Tozzi P., 1998, *ApJ*, 501, 493
 Cen R., Ostriker J. P., 1999, *ApJ*, 514, 1
 Croft R. A. C., Di Matteo T., Davé R., Hernquist L., Katz N., Fardal M. A., Weinberg D. H., 2001, *ApJ*, 557, 67
 da Silva A. C., Kay S. T., Liddle A. R., Thomas P. A., Pearce F. R., Barbosa D., 2001, *ApJ*, 561, L15
 Davé R., et al., 2001, *ApJ*, 552, 473
 De Luca A., Molendi S., 2004, *A&A*, 419, 837
 Di Matteo T., Springel V., Hernquist L., 2005, *Nat*, 433, 604
 Diaferio A., et al., 2005, *MNRAS*, 356, 1477
 Dolag K., Grasso D., Springel V., Tkachev I., 2005, *JCAP*, 1, 9
 Ebeling H., Edge A. C., Bohringer H., Allen S. W., Crawford C. S., Fabian A. C., Voges W., Huchra J. P., 1998, *MNRAS*, 301, 881
 Etori S., et al., 2004, *MNRAS*, 354, 111
 Finoguenov A., Briel U. G., Henry J. P., 2003, *A&A*, 410, 777
 Giacconi R., et al., 2002, *ApJS*, 139, 369
 Jubelgas M., Springel V., Dolag K., 2004, *MNRAS*, 351, 423
 Liedahl D. A., Osterheld A. L., Goldstein W. H., 1995, *ApJ*, 438, L115
 Markevitch M., et al., 2003, *ApJ*, 583, 70
 Moretti A., Lazzati D., Campana S., Tagliaferri G., 2002, *ApJ*, 570, 502
 Muanwong O., Thomas P. A., Kay S. T., Pearce F. R., Couchman H. M. P., 2001, *ApJ*, 552, L27
 Pearce F. R., Thomas P. A., Couchman H. M. P., Edge A. C., 2000, *MNRAS*, 317, 1029
 Raymond J. C., Smith B. W., 1977, *ApJS*, 35, 419
 Roberts T. P., Warwick R. S., 2001, in *ASP Conf. Ser. 234: X-ray Astronomy 2000* p. 569
 Rosati P., Borgani S., Norman C., 2002, *ARA&A*, 40, 539
 Rosati P., della Ceca R., Burg R., Norman C., Giacconi R., 1995, *ApJ*, 445, L11
 Rosati P., della Ceca R., Norman C., Giacconi R., 1998, *ApJ*, 492, L21
 Springel V., 2005, preprint, astro-ph/0505010
 Springel V., Hernquist L., 2003, *MNRAS*, 339, 289
 Springel V., White M., Hernquist L., 2001, *ApJ*, 549, 681
 Tornatore L., Borgani S., Matteucci F., Recchi S., Tozzi P., 2004, *MNRAS*, 349, L19
 Tornatore L., Borgani S., Springel V., Matteucci F., Menci N., Murante G., 2003, *MNRAS*, 342, 1025
 Tozzi P., Norman C., 2001, *ApJ*, 546, 63
 Voit G. M., 2005, *Reviews of Modern Physics*, 77, 207
 Voit G. M., Bryan G. L., 2001a, *ApJ*, 551, L139
 Voit G. M., Bryan G. L., 2001b, *Nat*, 414, 425
 Voit G. M., Bryan G. L., Balogh M. L., Bower R. G., 2002, *ApJ*, 576, 601
 White M., Hernquist L., Springel V., 2002, *ApJ*, 579, 16
 Worsley M. A., et al., 2005, *MNRAS*, 357, 1281
 Worsley M. A., Fabian A. C., Barcons X., Mateos S., Hasinger G., Brunner H., 2004, *MNRAS*, 352, L28
 Xue Y., Wu X., 2003, *ApJ*, 584, 34
 Zappacosta L., Mannucci F., Maiolino R., Gilli R., Ferrara A., Finoguenov A., Nagar N. M., Axon D. J., 2002, *A&A*, 394, 7